Available online at www.sciencedirect.com
SCIENCE @ DIRECT®
ELSEVIER
Journal of the European Ceramic Society 26 (2006) 1801–1805
ECERS
www.elsevier.com/locate/jeurceramsoc

Evanescent microwave probe study on dielectric properties of materials

Hsiu-Fung Cheng[a,*], Yi-Chun Chen[b], I-Nan Lin[c]

[a] *Department of Physics, National Taiwan Normal University, Taipei 116, Taiwan, ROC*
[b] *Department of Physics, National Cheng Kung University, Tainan 701, Taiwan, ROC*
[c] *Department of Physics, Tamkang University, Tamsui 251, Taiwan, ROC*

Available online 26 October 2005

Abstract

A recently developed evanescent microwave probe (EMP) technique combined with systematically quantitative analyses is demonstrated. We use a three-dimensional (3D) finite element simulation to model the electromagnetic field inside the resonant cavity and inside the sample near the tip. We also proposed an analysis model for the sample's quality factor (Q), which is usually hindered by the conductor losses of the resonator. Measurement on various dielectric samples agrees very well with the theoretical model, demonstrating the validity of analyses for the EMP resonator and providing a possibility for dielectric imaging the surface of the samples with high resolution.
© 2005 Published by Elsevier Ltd.

Keywords: Dielectric properties; Impurities; Surfaces; Evanescent microwave microscopy

1. Introduction

The improvement on microwave dielectrics is an important issue for the advanced communication technologies. However, the dielectric properties of materials are process-dependent. Extrinsic factors, such as defects (vacancies, impurities), structural disorder, porosity or second phases . . . etc., are formed during the synthesis process and need to be separated from the intrinsic ones to understand the dielectric mechanism for the materials. The difficulty in characterizing the materials' dielectric properties comes from the fact that the extrinsic structures are mostly of microscale sizes, which are far smaller than the wavelength in the microwave frequency region and can hardly be resolved by conventional microwave measurement techniques. Therefore, a specially designed probe for examining the microwave dielectric properties in the micrometer scale is urgently required.

Evanescent waves, which decay exponentially, have spatial frequency components higher than $1/\lambda$. Over the years, a variety of near-field scanning microscopes has been developed to probe local variations in the properties and structures of materials, attaining a spatial resolution of $\lambda/20$–$\lambda/600$.[1] Recently, Xiang et. al., demonstrated an evanescent microwave probe (EMP) with a spatial resolution to ∼50 nm by using a tip-probe structure.[2] This technique has been used to image surface the impedance profiles in various materials,[2–5] such as superconductors, ferroelectrics, magnetic materials and semiconductors. For EMP measurements on microwave dielectrics,[6–8] the improvement on the accuracy of quantitative analyses for dielectric properties is needed.

In this study, we used a three-dimensional (3D) finite element simulation and theoretical models to improve the accuracy of the analyses in EMP measuring technique. The validity of modeling was demonstrated by EMP measurements on different dielectric samples.

2. Experimental methods

The EMP system basically consists of a sharpened metal tip, which is mounted on the center conductor of a high quality factor (Q) $\lambda/4$ coaxial resonator, protruding beyond an aperture formed at the end wall of the resonator. A sapphire disk containing an aperture of size close to the diameter of the tip wire is coated with a metal layer (∼1 μm) on the disk outside surface, so as to shield the far-field propagating components and to improve spatial resolution. The resonator acts as both an evanescent field emitter and a detector. A change in the local environment near the probe leads to the variation in the EMP frequency response, which is used for deducing the dielectric properties of the materials adjacent to the probe. The frequency response of the EMP was analyzed using a lumped series resonant circuit, and tip-sample

* Corresponding author. Tel.: +886 229 331 075; fax: +886 229 326 408.
E-mail address: hfcheng@phy03.phy.ntnu.edu.tw (H.-F. Cheng).

0955-2219/$ – see front matter © 2005 Published by Elsevier Ltd.
doi:10.1016/j.jeurceramsoc.2005.09.034

interaction is simulated by the perturbation technique using a small complex capacitance, namely,

$$C_{\text{tip-sample}} = C_r + iC_i, \quad (1)$$

where C_r and C_i are the real and imaginary parts of the tip-sample capacitance, which are mainly contributed from the dielectric constant ε and dielectric loss tan δ (or $1/Q$) of the tested sample, respectively.

Due to the rapid decay of the evanescent wave, the tip-sample capacitance is far less than the resonator capacitance, such that the resonator can be analyzed by the perturbation theory. The complex tip-sample capacitance can be extracted from the measured resonant frequency f_r and quality factor Q:[9]

$$\frac{\Delta f}{f_0} = \frac{f_r - f_0}{f_0} = -\frac{C_r}{2C}, \quad (2)$$

$$\Delta\left(\frac{1}{Q}\right) = \frac{1}{Q} - \frac{1}{Q_0} = -\left(\frac{1}{Q_0} + \frac{2C_i}{C_r}\right)\frac{\Delta f}{f_0}, \quad (3)$$

where f_0 and Q_0 are the resonant frequency and quality factor of the resonator when there is no sample near the tip, respectively.

$Ba(Mg_{1/3}Ta_{2/3})O_3$ (BMT) and $Ba_2Ti_9O_{20}$ (B_2T_9) materials were chosen as standards to test the validity of the EMP measurements. The BMT materials were synthesized by traditional mixed-oxide process and sintered at 1550 °C for 4 h. The $Ba_2Ti_9O_{20}$ materials were prepared by the coprecipitation method, in which $Ba(OH_2)\cdot 2H_2O$ and $TiCl_4$ in appropriate ratio (Ba:Ti = 2:9) were dissolved in H_2O and then added into the coprecipitants consisting of $NH_4(OH)$ and $(NH_4)_2CO_3$ mixture. The coprecipitants thus obtained were filtered, washed several times to get rid of residual NH_4Cl and calcined at 1100 °C for 4 h, followed by pulverization, pressing and then sintering at 1200–1300 °C for 4 h. Three kinds of ambient gases, N_2, O_2 and air, were used during the calcining and sintering steps.

3. Results and discussion

To quantitatively extract the sample's dielectric properties from the measured EMP results, the relationship between the $C_{\text{tip-sample}}$ and the sample properties need to be determined. Gao and Xiang have proposed an approximate analytical model to solve C_r, which is directly related to the dielectric constant of the samples, by using the image charge theory,[9] in which, the tip was treated as a perfectly conducting sphere, and the quasi-static field distribution was assumed since the spatial extent of the sample-tip interaction depth was much less than the microwave wavelength. Such an assumption leads to a simple relationship between the dielectric constant of the samples and the EMP frequency shift of the resonator:

$$\frac{\Delta f}{f_0} = A\left[\frac{\ln(1-b)}{b} + 1\right], \quad (4)$$

where $b = (\varepsilon - \varepsilon_0)/(\varepsilon + \varepsilon_0)$; ε and ε_0 are the relative dielectric constants of the sample and vacuum, respectively. A is a constant related to the geometry of the tip-cavity assembly which should be calibrated using standard samples.

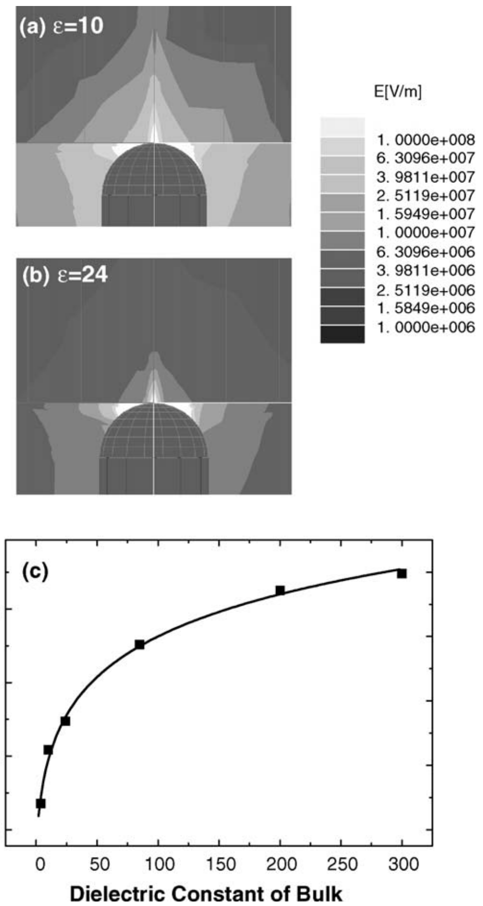

Fig. 1. Simulated electric field distribution from the EMP tip to the sample with dielectric constants (a) $\varepsilon = 10$ and (b) $\varepsilon = 24$; (c) the frequency shift derived by HFSS simulation (solid squares) and the frequency shift vs. dielectric constant curve fitted using formulas derived by perturbation model (tip radius: $R_0 \sim 35$ μm).

To verify the accuracy of the approximate analytical model, the field distribution and frequency response of the EMP resonator were solved numerically by a finite element method using a software package (3D Ansoft HFSS, v. 8). The typical simulation results, which show the near-field distribution around the tip and inside the sample, are presented in Fig. 1(a) and (b) for a sample with $\varepsilon = 10$ and 24, respectively. These figures clearly indicate that the sharp tip enhances the concentration of the electric field. Only a very small volume of the sample near the tip interacts with the evanescent field, such that the measuring system can have a very high spatial resolution. It should be noted that the field intensity propagating out of the resonator decays exponentially and can only penetrate into the material for about 10–100 μm, depending on the dielectric constant of the sample. The field distribution shown in Fig. 1(a) and (b) indicates that the field inside the high dielectric constant sample is more concentrated and penetration is shallower. In general, the spatial resolution for a tip with radius of tens of microns is about submicron.

The amount of simulated frequency shift ($\Delta f/f$) increases with the dielectric constant of the samples (solid squares, Fig. 1(c)). These numerically solved data were fitted by Eq. (4) to obtain

the "*A*" parameter, and the variation of frequency shift ($\Delta f/f$) with the dielectric constant of the samples is then shown as the continuous curve in Fig. 1(c). The perturbation model fits very well with the numerically simulation results, revealing that the approximate model not only applies to samples with low ε-values, but also is suitable for analyzing the high ε samples, such as ferroelectrics. From the theoretical result shown in Fig. 1(c), we can estimate that, with a low-noise microwave system, the sensitivity of the dielectric constant ($\Delta\varepsilon/\varepsilon$) is within 1% for the samples with $\varepsilon = 1$–100.

To demonstrate the capability of the EMP technique for detecting the microscale secondary phases, the BMT and B_2T_9 ceramic examples were examined. The B_2T_9 ceramics contain a large proportion of $BaTi_4O_9$ intermediate phase, whereas the BMT samples contain $Ba_5Ta_4O_{15}$ secondary phases, which were revealed by X-ray diffraction (not shown). Fig. 2(a) and (b), respectively, show the distribution of the dielectric constant, the dielectric mappings of B_2T_9 and BMT samples derived from EMP measurements. These mappings reveal that the average dielectric constant for B_2T_9 sample is around 32–33 and for the BMT sample is around 25–26, which are consistent with the dielectric properties measured by the conventional cavity method. Fig. 2(a)-I and (b)-I show that the dielectric constant of the materials is not uniformly distributed. There exist regions with higher or lower dielectric constants, which apparently results from the presence of secondary phases in these samples. Such a phenomenon is even more clearly illustrated in Fig. 2(a)-II and 2(b)-II, which show the high-resolution EMP mapping of the low ε region on the B_2T_9 and BMT samples, respectively. The dielectric constant varies pronouncedly over this region. Grains with low dielectric constant aggregate, forming clusters about tens of microns in size.

In B_2T_9 images, the low ε region contains several equiaxed clusters about tens of microns, and the high ε region consists of needle-like clusters, about 1 μm in diameter and several tens of microns in length. The needle-like clusters are most probably $Ba_2Ti_9O_{20}$ grains, whereas the equiaxed clusters are the secondary phases. In contrast, the fluctuation of the dielectric constants for the clusters in Fig. 2(b)-II can be attributed to the presence of a large proportion of $Ba_5Ta_4O_{15}$ secondary phase. These results illustrate that EMP is a useful tool for examining the extrinsic dielectric defects with high spatial resolution.

The analysis of the sample dielectric losses ($1/Q_d$) is much more complex. The most important factor inducing the complication is the conductor loss of the resonator dominating the measured quality factor Q of the resonator. Because of the extra current caused by the charge redistribution of the resonator at different frequencies, the effect of the resonator losses on the measurement is also varying with the dielectric properties of the samples. To extract the quality factor information of the samples from the measured frequency response of the resonator, we need to modify Eq. (3) by considering such a frequency-dependent variable. A parameter "*B*" is introduced in the first term of Eq. (3) to include the additional conductor losses, whereas another parameter "*B′*" is introduced in the second term by assuming that the equivalent C_i/C_r is proportional to the dielectric loss, $\tan\delta$, of the samples. The dielectric losses of the samples are thus correlated to the frequencies of the resonators by the following equation:

$$\Delta\left(\frac{1}{Q}\right) = -\left(\frac{B}{Q_0} + B' \tan\delta\right)\frac{\Delta f}{f_0}, \tag{5}$$

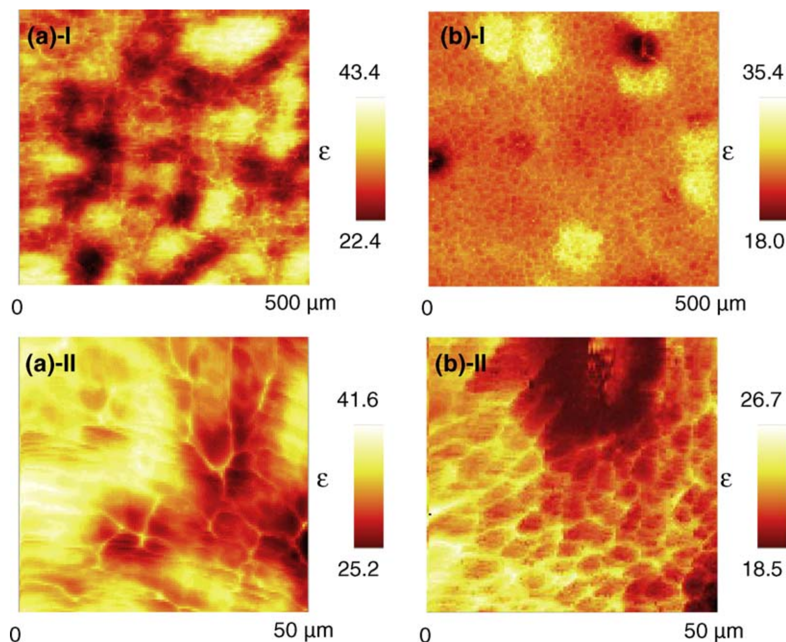

Fig. 2. Mappings of the dielectric constants for the secondary phase region in (a) B_2T_9 samples and (b) BMT samples (I, EMP scanned range 500 μm × 500 μm; II, EMP scanned range 50 μm × 50 μm).

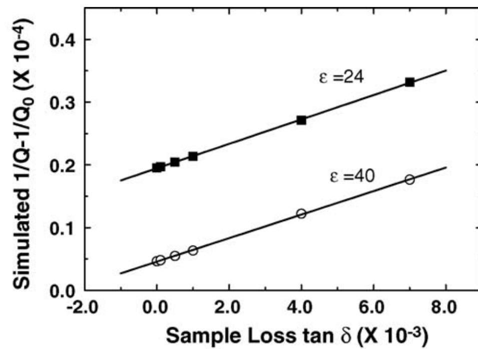

Fig. 3. Simulated change of quality factor ($1/Q$–$1/Q_0$) of EMP resonator vs. the sample losses (tan δ) (the quality factor of original resonator $Q_0 = 809$).

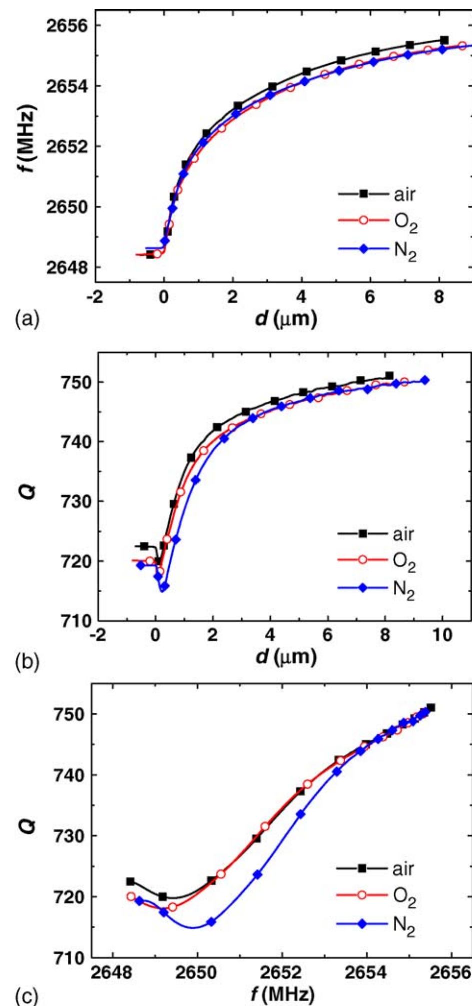

Fig. 4. (a) Resonant frequency approaching curves and (b) quality factor approaching curves, which were taken when the tip approached the B_2T_9 samples (d: tip-sample distance); (c) quality factor vs. resonant frequency (Q–f) curves of B_2T_9 samples during the approaching processes.

To investigate the behaviors of "B" and "B'", simulating the frequency response of the resonators with a series of samples having the same dielectric constant but with different dielectric losses is necessary. Fig. 3 shows the variation of the simulated quality factor change ($\Delta(1/Q)$) of the EMP resonator with the dielectric losses of the samples by using computer simulation. When the resonant frequency is fixed due to the same dielectric constants of the samples, the inverse of the quality factor change ($\Delta(1/Q)$) increases linearly with the sample losses, i.e., the "B" and "B'" parameters are constant. Fig. 3 shows that the fitted parameters are $B = 6.82$, $B' = 0.93$ and $B = 1.60$, $B' = 0.80$, for the samples with dielectric constants $\varepsilon = 24$ and 40, respectively. It is interesting to notice that the parameter "B'" is more stable than "B" and shifts only slightly with the samples. Therefore, we can easily determine the "B'" parameter by using the standard samples in the experiment.

The sensitivity of the dielectric loss measurement is limited by the conductor loss of the resonator. Fig. 3 revealed that the change of the measured Q is higher than 1% only when the dielectric loss of the sample is larger than 10^{-3}, which is about the same order of the resonator's conductor loss. Therefore, the linear fit analysis described earlier is only applicable for sample with tan δ larger than 10^{-3}. However, since the noise-limited sensitivity in our system is quite high ($\Delta f_r/f_r = 10^{-6}$**)**, the measured variation due to the dielectric loss can be highly improved if we can subtract the "B"-term effect from Eq. (5) systematically. To reveal the frequency dependence of "B" parameters, we perform the tip-approaching measurement on high-Q B_2T_9 materials. Fig. 4(a) and (b) illustrate, respectively, the change in the resonance frequency and the resonator quality factor curves as the tip gradually approaches the B_2T_9 surface, which were designated as f- and Q-approaching curve, respectively. The B_2T_9 samples are synthesized in three different ambient gases, N_2, O_2 and air, and possess similar dielectric constant but with pronouncedly different $Q_d \times f$-values, i.e., $\varepsilon_{N_2} = 36.3$, $(Q_D \times f)_{N_2} = 28,200$; $\varepsilon_{O_2} = 38.6$, $(Q_D \times f)_{O_2} = 31,200$; $\varepsilon_{air} = 38.7$, $(Q_d \times f)_{air} = 30{,}500$. It is also noticeable that the effect of the air gap between the tip and the sample will cause pronounced change in the resonant frequency (f) and quality factor (Q). Therefore, when performing surface response imaging, a soft tape cantilever combined with a piezo-feedback system was used to hold the sample soft contact with the tip during scanning. By using such a technique, the height control can be maintained within the nanometer range, which only causes frequency change ratio ($\Delta f_r/f_r$) $\sim 10^{-6}$ and quality factor change ratio ($\Delta Q/Q$) $\sim 10^{-5}$. The topography effect is thus minimized. Fig. 4(a) and (b) indicate that the f-approaching curves remained almost the same for the three samples, whereas the Q-approaching curves of the samples deviate from each other significantly.

Fig. 4(c) shows the variation of Q against the resonant frequency (f) during the approaching process (Q–f). Since the dielectric losses of the B_2T_9 samples ($\sim 10^{-4}$) are markedly smaller than the conductor loss of the resonator ($\sim 2 \times 10^{-3}$), the variation of the approaching curves in Fig. 4(c) is dominated by the "B" term in Eq. (5). For B_2T_9 samples sintered in O_2 and air, which have nearly the same dielectric constants, the Q–f curves are almost overlapped, except for the case when the tip contacts the sample. The overlapped parts imply the comparable "B" parameters for these two approaching measurements, and the difference at the contact point may mainly come from the discrepancy of the sample losses. The deviation of the approaching

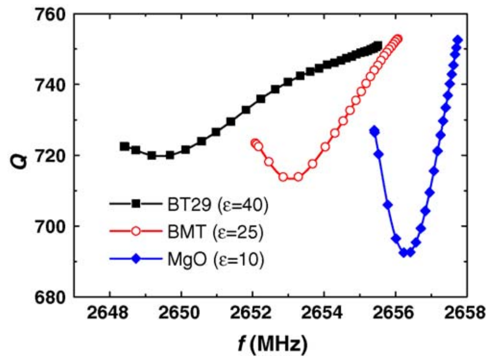

Fig. 5. Quality factor vs. resonant frequency (Q–f) curves taken when tip approached the B_2T_9, BMT or MgO samples.

curves for B_2T_9 synthesized in N_2 gases with those of the other two curves indicate that the "B" parameter is very sensitive to the dielectric constant of the sample. The phenomenon comes from the resonant-like variation of the Q–f curve when the tip-sample distance is smaller than 1 μm. The most probable explanation of this variation is the change of input/output coupling to the resonator. The minimum measured Q-value should correspond to the strongest coupling, where the field distribution makes the impedance of the whole system relatively matched to the external circuits.

The resonant-like variation is also shown in the various samples. Fig. 5 shows the comparison of Q–f curves while the tip approaches the MgO, BMT or B_2T_9 samples. The frequency for the minimum quality factor increases and the variation becomes more pronounced when the sample has lower dielectric constant. Since the unsteadiness of the "B" parameter mainly results from the resonant-like variation, the impedance matching design of the resonator and external circuits is a key factor for improving the dielectric-loss measurement. A resonator filling with lower dielectric constant material can reduce the resonant-like variation. However, more simulated data are needed for establishing a suitable model of the resonant-like variation, which will be performed in the near future.

4. Conclusions

The quantitative analyses of EMP resonator are demonstrated. The dielectric constants of the samples under test can be derived from the shift of the resonant frequencies, which were properly modeled by theory, and proved by a three-dimensional (3D) finite element simulation. Thus, obtained dielectric constants are consistent with those obtained from the conventional cavity measurement. A systematical way for analyzing the dielectric losses is also proposed. The results reveal that the EMP technique possesses good potential for overcoming the conventional measurement limit. A submicron spatial resolution is achieved in the dielectric images, showing that the EMP technique is useful for studying the extrinsic microwave dielectric properties of the materials in the microscale region.

Acknowledgement

Financial support of National Science Council, ROC, through the project NSC-93-2112-M-003-011 and NSC-94-2112-M-006-011 are gratefully acknowledged by the authors.

References

1. Lahrech, A., Bachelot, R. P., Gleyzes and Boccara, A. C., Infrared near-field imaging of implanted semiconductors: evidence of a pure dielectric contrast. *Appl. Phys. Lett.*, 1997, **71**, 575–577.
2. Lu, Y., Wei, T., Duewer, F., Lu, Y., Ming, N. B., Schultz, P. G. *et al.*, Nondestructive imaging of dielectric-constant profiles and ferroelectric domains with a scanning-tip microwave near-field microscope. *Science*, 1997, **276**, 2004–2006.
3. Takeuchi, I., Wei, T., Duewer, F., Yoo, Y. K., Xiang, X. D., Talyansky, V. *et al.*, Low temperature scanning-tip microwave near-field microscopy of YBCO films. *Appl. Phys. Lett.*, 1997, **71**, 2026–2028.
4. Gao, C., Duewer, F. and Xiang, X. D., Quantitative microwave evanscent microscopy. *Appl. Phys. Lett.*, 1999, **75**, 3005–3007.
5. Duewer, F., Gao, C. and Xiang, X. D., Tip-sample distance feedback control in a scanning evanescent microwave probe for nonlinear dielectric imaging. *Rev. Sci. Instrum.*, 2000, **71**, 2414–2417.
6. Cheng, H.-F., Chen, Y.-C., Wang, G., Xiang, X.-D., Chen, G.-Y., Liu, K.-S. *et al.*, Study of second-phase effects in $Ba(Mg_{1/3}Ta_{2/3})O_3$ materials by microwave near-field microscopy. *J. Eur. Ceram. Soc.*, 2003, **23**, 2671–2675.
7. Chen, Y.-C., Hsieh, Y.-S., Cheng, H.-F. and Lin, I.-N., Study of microwave dielectric properties of perovskite thin films by near-field microscopy. *J. Electroceram.*, 2004, **13**, 261–265.
8. Chen, Y.-C., Cheng, H.-F., Wang, G., Xiang, X.-D., Lei, C.-M. and Lin, I.-N., Measurement of dielectric property by evanescent microwave microscope. *Jpn. J. Appl. Phys.*, 2002, **41**, 7214–7217.
9. Gao, C. and Xiang, X. D., Quantitative microwave near-field microscopy of dielectric properties. *Rev. Sci. Instrum.*, 1998, **69**, 3846–3851.